THE JOURNAL OF PHYSICAL CHEMISTRY C
A JOURNAL OF THE AMERICAN CHEMICAL SOCIETY

pubs.acs.org/JPCC
Article

Exploring the Interaction of Water with Open Metal Sites in MIL-101(Cr) by ^{1}H NMR Relaxometry and ReaxFF Molecular Dynamics Simulations

Francesca Martini, Lucia Calucci, Larisa G. Gordeeva, Susanna Monti, Marina V. Solovyeva, Cheherazade Trouki, and Silvia Pizzanelli*

Cite This: https://doi.org/10.1021/acs.jpcc.3c03901
Read Online

ACCESS | Metrics & More | Article Recommendations | Supporting Information

ABSTRACT: In this work, we investigated the state of water in the metal−organic framework MIL-101(Cr) by combining ^{1}H magic angle spinning (MAS) NMR, NMR relaxometry, and molecular dynamics (MD) simulations based on a reactive force field. The MD simulations indicated that water molecules are coordinated to the open metal sites and are organized in shells. Through ^{1}H T_2 and T_1 relaxation measurements at the fixed Larmor frequency of 21 MHz, water in the intergrain spaces was distinguished from that in the intragrain mesopores of MIL-101(Cr). ^{1}H MAS NMR measurements showed that water in the mesopores is structurally ordered, as revealed by the presence of ^{1}H−^{1}H residual dipolar interaction. The ^{1}H NMR relaxometric behavior of water located in the intergrain spaces of MIL-101(Cr) as a function of the magnetic field strength, determined by fast field cycling NMR relaxometry, was interpreted extending an existing model, generally applied to paramagnetic aqua ions in solution, to the case of Cr^{3+} ions fixed on the surface of the metal−organic framework. The model predicts the exchange of water between the first and second shell of a Cr^{3+} ion, giving access to the water residence time in the first shell that would be difficult to determine using other techniques. In the temperature interval of 25−70 °C, water residence times in the range of tens of nanoseconds were found and a limited accessibility of water to the open metal sites located on the external grain surface was observed.

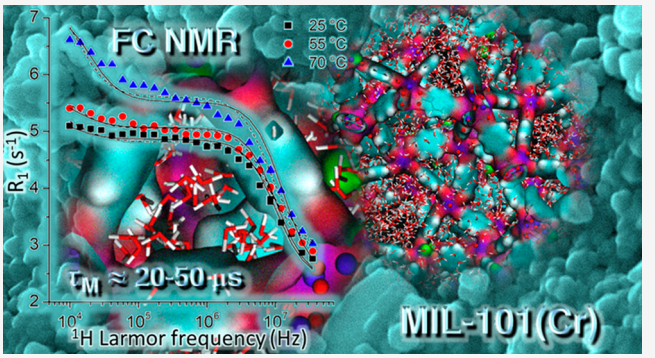

1. INTRODUCTION

Metal−organic frameworks (MOFs) are crystalline porous materials made of metal clusters and organic ligands. The pores' size, shape, and accessibility can be finely tuned by changing the type of metal and/or ligand. These materials are receiving considerable attention not only for their structural properties but also for their functional features. The presence of Lewis acid sites, which are either framework defects or coordinatively unsaturated metal sites (CUSs, also referred to as open metal sites), plays an essential role in the adsorptive removal of hazardous materials[1] and in heterogeneous catalysis.[2−4] MIL-101(Cr) (formula $Cr_3O(H_2O)_2F(BDC)_3$ with BDC = 1,4-benzene dicarboxylate), one of the most studied MOFs,[5] was capable of removing various nitrogen-containing compounds from fuels[6−9] and was also tested as a heterogeneous catalyst in many reactions where its open metal sites were involved.[10−14] MIL-101(Cr) contains inorganic trimers consisting of three chromium ions in an octahedral environment. In a trimer, each Cr^{3+} ion is connected to four oxygen atoms of the organic linker and one μ_3-O atom. In the sixth site of the octahedral coordination, two of the three Cr atoms are bound to a water oxygen, and the other to a fluorine atom. Water molecules can be removed, creating CUSs. The linkage of the BDC anions with the trimers defines a super tetrahedral unit with the trimers at the four vertices and the organic linkers at the six edges. The super tetrahedra define a 3D structure with micropores (diameter of 8 Å) and two types of interconnected mesoporous cages (diameters of 29 and 34 Å) (Figure 1).

Although the CUSs are involved in many applications,[1−4,6−14] the guests' behavior at MIL-101(Cr) open metal sites is not entirely understood. The interactions of a water molecule and some N-donor molecules with CUSs within MIL-101(Cr) were investigated by solid-state NMR, and a binding preference scale was defined based on competition experiments.[15] It was found that guest molecules

Received: June 9, 2023
Revised: August 19, 2023

https://doi.org/10.1021/acs.jpcc.3c03901
J. Phys. Chem. C XXXX, XXX, XXX−XXX

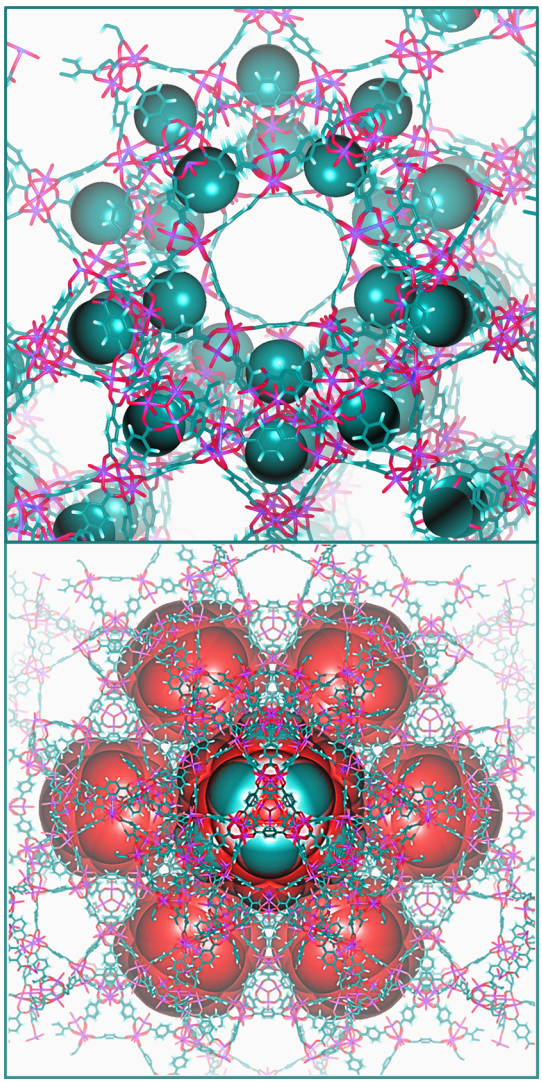

Figure 1. Crystal structure of MIL-101(Cr) showing the micropores (8 Å – top image) and the mesoporous medium (29 Å – bottom image: the smaller six red spheres surrounding the central sphere) and large (34 Å – bottom image: large red sphere in the center of the model) cages. Color code: Cr, violet/magenta; C, dark cyan; O, red; H, white; F, green.

may induce somewhat peculiar effects. For example, water, acetonitrile, *tert*-butanol, and pyridine coordinated to the open metal sites increased the MIL-101(Cr) framework mobility.[16] Instead, the mobility of molecules bound to the open metal sites, in particular, their lifetime within the metal coordination shell, was rarely investigated. Over the years, this aspect was extensively discussed for solvent molecules coordinated to metal ions in solution.[17] Similarly to the ions in solution, water molecules are expected to affect the metal ions' reactivity in the MOF framework as well. This issue was addressed only in the case of pyridine interacting with the MIL-100(Al) open metal sites.[18]

In the present work, we focus on the mobility of the water molecules coordinated to the CUSs of MIL-101(Cr). In a previous study,[19] Gao et al. characterized the state of water confined in MIL-101(Cr) using infrared spectroscopy and molecular dynamics (MD) simulations based on the RASPA approach,[20] which was appropriately developed for reproducing the adsorption and diffusion of molecules in flexible porous materials. Their nonreactive simulations with fixed parameters (such as atomic charges and bonds) were focused on the motion and localization of water molecules at different water loadings to interpret the primary vibrations responsible for the dominant peaks of DRIFTS spectra. For this reason, they had to choose a very small time step (0.05 fs) and limit the simulation time to 25 ps. They could successfully and elegantly identify the positions of all of the water molecules, including those bound to CUSs, but neglected their speciation and subtle dynamics that could be crucial for the guest motions and the catalytic efficiency of the framework.

Here, we move a step forward by combining reactive MDs (extended to 500 ps) based on a tuned force field (with variable charges, responding to the local environment), capable of disclosing bond breaking and formation, with ^{1}H NMR spectroscopy and relaxometry to reveal the details of the water motions. ^{1}H magic angle spinning (MAS) NMR spectroscopy revealed the presence of structured water close to the mesopore surface (but not water bound to Cr), in agreement with MD simulations. This type of water is in fast exchange with "bulk" water located in the inner part of the pore. On the other hand, ^{1}H NMR relaxometry as a function of the magnetic field strength (specifically ^{1}H fast field cycling (FFC) NMR relaxometry) pointed to the presence of water bound to CUSs and gave insight into the exchange between the first and the second coordination shell of the Cr ion by exploiting paramagnetic relaxation enhancement.[21] This peculiar technique is often employed to evaluate the local chemical environment of paramagnetic centers and their interaction with water molecules in solution and only in a few cases was applied to paramagnetic MOFs,[22,23] although it is not limited to them.[24] Here, FFC NMR relaxometry allowed us to effectively assess the lifetime of water on the MIL-101(Cr) open metal sites together with the accessibility to water of these sites.

This work is organized as follows. First, details on the samples' preparation are presented, together with the procedures adopted in the MD simulations and NMR data acquisition and analysis. Then the MD results concerning atomic distances and porosity are discussed and evidence on the water structuring in the mesopores collected by ^{1}H NMR is presented. In the following section, water in the intergrain spaces was distinguished from that in the intragrain mesopores of MIL-101(Cr) using ^{1}H T_2 and T_1 relaxation measurements at the fixed Larmor frequency of 21 MHz. It was necessary to distinguish the water in the two compartments to set the conditions to be applied in the successive ^{1}H FFC NMR experiments, where we chose to selectively probe water molecules located in the intergrain spaces of the MOF. In the last part of the work, the nuclear magnetic relaxation dispersion (NMRD) profiles of a wet MIL-101(Cr) sample in the temperature range of 25−70 °C are displayed and interpreted.

2. MATERIALS AND METHODS

2.1. Samples. *2.1.1. Preparation and Characterization of MIL-101(Cr).* MIL-101(Cr) was synthesized according to the procedure described in ref 25, and it was characterized by X-Ray powder diffraction (Figure S1), nitrogen adsorption measurements (Table S1), water adsorption measurements (Figure S2), scanning electron microscopy (SEM) (Figure S3), and ^{1}H MAS NMR spectroscopy (Figures S4 and S5).

https://doi.org/10.1021/acs.jpcc.3c03901
J. Phys. Chem. C XXXX, XXX, XXX−XXX

2.1.2. Preparation of the Samples Studied by ^{1}H MAS NMR and ^{1}H NMR Relaxometry. Dry MIL-101(Cr) was prepared by heating the powder at 120 °C for 4 h in order to remove water that was not bound to the coordinatively unsaturated metal sites. MIL-101(Cr) with a hydration degree of 45 wt % (MIL-101(Cr)-45w) was obtained by exposing dry MIL-101(Cr) to a humid atmosphere at room temperature. The hydration degree, measured gravimetrically, is defined as the ratio $\frac{m_1}{m_1+m_2} \times 100$, where m_1 and m_2 represent the mass of the adsorbed water and that of dry MIL-101(Cr), respectively. Dry MIL-101(Cr) and MIL-101(Cr)-45w were studied by ^{1}H MAS NMR, and the latter sample was also studied with NMR relaxometry.

The other samples studied by NMR relaxometry were prepared by mixing weighted amounts of dry MIL-101(Cr) with known volumes of ultrapure water (MilliQ; 18.2 MΩ cm at 25 °C). In the wet powder samples, the amount of water ranged from 68 to 90 wt %. These samples are indicated as MIL-101(Cr)-Xw, where X represents the weight percentage of water.

2.2. ReaxFF Molecular Dynamics Simulations. The crystallographic information file (cif format) for MIL-101(Cr) was downloaded from the Cambridge Crystallographic Data Centre, entry CCDC: OCUNAC 605510 (catena-[tris(μ_4-Terephthalato)-(μ_3-oxo)-diaqua-fluoro-trichromium pentadecahydrate]). Space Group: Fd3m (227), Cell: a 88.87 Å, b 88.87 Å, c 88.87 Å, α 90°, β 90°, γ 90°.[26,27] We removed the 34 water molecules in the cif file and added all of the hydrogens and a fluorine atom to the inorganic trimers. Then we energy-minimized the structure with a reactive force field-based method (ReaxFF) used in an earlier investigation.[28] As a second step, we filled the final optimized configuration with water molecules using repeated water insertions followed by low-temperature (T = 250 K) MD equilibrations in the NVT ensemble. Approximately 18300 water molecules were inserted in the simulation box. During the filling process, we observed the same behavior described by Gao et al.,[19] and after equilibration, we found that the average number of water molecules inside the 8 Å cages was six. After reaching an almost *uniform* distribution of the water molecules among the mesoporous cages, we used the last sampled equilibrated structure as starting configuration of NVT MD at T = 298 K to investigate water dynamics and adsorption in the various MOF portions (the solvated model is shown in Figure S6). We performed all MD simulations with the Amsterdam density functional (ADF)/ReaxFF implementation.[29] Reactivity was always on to disclose water dissociation and the evolution of the connection of the various species to the Cr^{3+} ions, and no constraints were applied to the system. All of the species could interact with each other and modify their arrangements/nature in response to the local environment. Production MDs were carried out in the NVT ensemble for about 500 ps, the time step was set to 0.2 fs, and the temperature was controlled through the Anderson thermostat with a relaxation constant of 0.1 ps. Periodic boundary conditions were applied in all directions, the system structures were collected every 0.02 ps, and the last 100 ps of the trajectory, reliably representing the MOF dynamics, was used for the final analysis. The reported descriptors are mainly atom−atom radial distribution functions (RDFs) and atom−atom distances. However, visual inspection of the trajectories was fundamental to understanding water motion and adsorption on the framework portions.

2.3. NMR Data Acquisition and Analysis. *2.3.1. ^{1}H MAS NMR.* ^{1}H MAS NMR experiments were carried out on a Bruker Avance Neo-500 NB spectrometer operating at 500.13 MHz and equipped with a Bruker 1.3 mm double resonance probe. The 90° pulse duration and the recycle delay were set to 1.5 μs and 3 s, respectively, and 64 scans were accumulated. Spinning rates of 20 and 67 kHz were used.

2.3.2. ^{1}H NMR Relaxometry at 21 MHz. ^{1}H time domain NMR measurements were performed at 21 MHz using a low-field NMR spectrometer constituted of a Niumag permanent magnet interfaced with a Stelar PC-NMR console. The ^{1}H 90° pulse duration was 3.3 μs. Transverse relaxation curves were recorded for all the wet powder samples using the Carr-Purcell-Meiboom-Gill (CPMG) pulse sequence.[30] The long decaying component was extracted from data acquired with a time between successive 180° pulses ranging between 500 μs and 1 ms, depending on the sample, whereas the short decaying component was extracted from data acquired with a time between successive 180° pulses of 50 μs. In both cases, the total number of 180° pulses was 2048, and the number of transients was 16. T_1 relaxation times were obtained by applying the standard inversion recovery pulse sequence under on-resonance conditions. The magnetization intensity for each value of the variable delay was taken from the average of all of the points collected in the free induction decay (FID). The recovery was described using 24 recovery delays, and 4 transients were accumulated for each delay. For all of the experiments, a recycle delay of 3 s was used. The temperature was controlled with a variable temperature controller and set to 25 °C. Relaxation times were obtained from the relaxation curves employing nonlinear least-squares fit routines.

2.3.3. ^{1}H Fast Field Cycling NMR Relaxometry. The ^{1}H T_1 values were measured in the 0.01−35 MHz Larmor frequency range using a Stelar SpinMaster FFC-2000 fast field cycling NMR relaxometer to obtain NMRD curves. The experiments were performed using the prepolarized and non-prepolarized pulse sequences below and above 12 MHz, respectively. The polarizing and detection fields were 0.60 and 0.50 T, corresponding to ^{1}H Larmor frequencies of 25.0 and 21.5 MHz, respectively. The switching time was 3 ms, and the 90° pulse duration was 9.8 μs. The dead time was 14.5 μs. A single scan was acquired. All of the other experimental parameters were optimized for each measurement. All of the ^{1}H magnetization curves vs time were monoexponential within experimental error, and the errors on the relaxation rates R_1 (= $1/T_1$) obtained from the fitting of the curves were always lower than 1%. Measurements were performed in the temperature range of 25−70 °C. The temperature was controlled within ±0.1 °C with a Stelar VTC90 variable temperature controller.

2.3.4. Theoretical Model for the Analysis of the FFC NMR Data. The longitudinal relaxation of water protons in the MIL-101(Cr)-90w sample was modeled considering two phases in fast exchange one with the other: a liquid phase affected by surface effects and a bulk liquid phase.[31−35] In the surface-affected liquid phase, water molecules either belong to the coordination sphere of Cr^{3+} paramagnetic centers, where they are characterized by the longitudinal relaxation time T_{1param}, or diffuse on the surface around such centers, where they are characterized by T_{1surf}. It must be noticed that the possible contribution to relaxation arising from reorientations of water molecules on the MOF surface without paramagnetic species was considered negligible with respect to those from water molecules interacting with Cr^{3+} paramagnetic centers, as

https://doi.org/10.1021/acs.jpcc.3c03901
J. Phys. Chem. C XXXX, XXX, XXX−XXX

usually done.[31−36] In the bulk liquid phase, ^{1}H longitudinal relaxation is characterized by the relaxation time T_{1bulk}, which is determined by the fast and isotropic tumbling of water molecules. In the fast diffusion limit between the two phases, the overall ^{1}H spin lattice relaxation rate, $1/T_1$, is given by the following equation:

$$\frac{1}{T_1} = \frac{N_{param}}{N}\frac{1}{T_{1param}} + \frac{N_{surf}}{N}\frac{1}{T_{1surf}} + \frac{N_{bulk}}{N}\frac{1}{T_{1bulk}} \quad (1)$$

where $\frac{N_{param}}{N}$ is the fraction of water molecules directly bound to Cr^{3+}, $\frac{N_{surf}}{N}$ is the fraction of water molecules on the pore surface and not bound to Cr^{3+}, and $\frac{N_{bulk}}{N}$ is the fraction of the bulk water molecules.

The contribution of bulk water protons, $1/T_{1bulk}$, arising from the modulation of ^{1}H−^{1}H dipolar interactions by molecular reorientation and fast translational diffusion motions in the frequency regime investigated by FFC NMR relaxometry, was considered to be frequency independent. In the literature, the contributions to relaxation of protons from water bound to $(1/T_{1param})$ or diffusing in proximity of $(1/T_{1surf})$ paramagnetic ions have been expressed using different models.[31−37] In particular, in a model devised by Korb, $1/T_{1surf}$ shows a bilogarithmic trend as a function of Larmor frequency and typically decreases when the temperature increases.[32,34,35] The well-known Bloembergen-Morgan theory of water relaxation in the presence of dissolved ions[38] has been used to model $1/T_{1param}$ of water confined in rocks containing Mn^{2+},[32−34] leading to a double Lorentzian trend, where the two components are given by the respective contributions at the nuclear and electron Larmor frequencies.

Since the observed NMRD profiles did not clearly exhibit any bilogarithmic trend and R_1 increased upon increasing the temperature, the $1/T_{1surf}$ contribution was deemed not to significantly affect the profiles and was assumed frequency-independent. On the other hand, the $1/T_{1param}$ contribution was considered dominant and, on the basis of Bloembergen-Morgan theory, was expressed as

$$\frac{1}{T_{1param}} = \frac{1}{T_{1Cr} + \tau_M} \quad (2)$$

where T_{1Cr} is the relaxation time of a water molecule bound to Cr^{3+}, and τ_M is the residence time of a water molecule in the coordination sphere of Cr^{3+}. This equation holds if N_{param}/N is much smaller than 1, a condition that was satisfied by the sample under examination, as outlined in Section 3.4. Considering that the dipolar interaction between a water proton and the chromium electrons is responsible for the relaxation of the bound water molecule, the relaxation rate $1/T_{1Cr}$ is given by the following expression:[21]

$$\frac{1}{T_{1Cr}} = \frac{2}{15}\left(\frac{\mu_0}{4\pi}\right)^2 \frac{\gamma_H^2 g^2 \mu_B^2 S(S+1)}{r_{CrH}^6}\left(\frac{3\tau_{d1}}{1+\omega_H^2\tau_{d1}^2} + \frac{7\tau_{d2}}{1+\omega_S^2\tau_{d2}^2}\right) \quad (3)$$

where r_{CrH} represents the distance between Cr^{3+} and the hydrogen atoms of the bound water. The correlation times τ_{d1} and τ_{d2} depend on the electron relaxation times T_{1e} and T_{2e}, respectively, and on τ_M according to the equation:

$$\frac{1}{\tau_{di}} = \frac{1}{T_{ie}} + \frac{1}{\tau_M} \text{ with } i = 1,\ 2 \quad (4)$$

It must be noted that τ_{d1} and τ_{d2} are not dependent on the overall reorientation of the Cr−H vector, as for paramagnetic aqua ions in solution, since Cr^{3+} ions are fixed on the surface. The field dependence of the electron relaxation has been described for $S = 3/2$ considering the modulation of the transient zero-field splitting (ZFS) as a result of collisions with solvent molecules.[39] The averaged longitudinal and transverse electron relaxation rates for the various nondegenerate transitions are expressed by the following equations:[40]

$$\frac{1}{T_{1e}} = \frac{1}{25}\Delta^2\tau_v[4S(S+1) - 3]\left[\frac{1}{1+\omega_S^2\tau_v^2} + \frac{4}{1+4\omega_S^2\tau_v^2}\right] \quad (5)$$

$$\frac{1}{T_{2e}} = \frac{1}{50}\Delta^2\tau_v[4S(S+1) - 3]\left[\frac{5}{1+\omega_S^2\tau_v^2} + \frac{2}{1+4\omega_S^2\tau_v^2} + 3\right] \quad (6)$$

where Δ^2 is the mean squared fluctuation of the ZFS of the Cr^{3+} ion and τ_v is the correlation time associated with the modulation of the ZFS interaction.

3. RESULTS AND DISCUSSION

3.1. Water in MIL-101(Cr) by Molecular Dynamics Simulations. Before analyzing the organization of the water molecules around the Cr^{3+} ions obtained through the MD simulations, we checked the effects of the system solvation on the framework structure by comparing the positions (RDF plots) of Cr^{3+} ions in the crystallographic geometry to those observed during the dynamics (Figure S7). Furthermore, we examined the relative locations of the coordinated COO^- oxygen atoms and their possible interactions with the water molecules nearby (Figure S8). The trends of both RDFs suggest that water did not perturb the MOF configuration substantially. The framework was stable and did not deviate much from the original model. Most of the water molecules remained far from the carboxylic groups, at a distance between a water hydrogen, HW, and an oxygen of the carboxylate group, O(COO), of about 2.15 Å (Figure S8). Only a few water molecules could reach the carboxyl moieties and slightly influence their dynamics through intermolecular hydrogen bonds and, sometimes, hydrogen transfers. These events, evidenced by the low peak at about 1 Å in the O(COO)−HW (water hydrogen) RDF in Figure S8, were sparsely populated and thus ineffective on the MOF configuration.

The Cr−OW (water oxygen) RDF plot (Figure 2, top) shows peaks at about 2.0, 4.2, and 5.4 Å, clearly indicating definite water shells around the Cr^{3+} ions. The separation of the first from the second peak by a zero-plateau reveals that no water exchange between the first and the second water layer (in the 3.2−4.8 Å distance range) takes place in the simulated time-span (500 ps). On the contrary, the RDF large intensity between the second and third peaks suggests water exchange. This is evident in the lifetime distribution of the water molecules in the second layer, as determined considering the last 100 ps of the MD trajectory. Indeed, the lifetimes of the molecules in the second layer were shorter than 12 ps (Figure S9). A finer analysis of the first peak disclosed a partial overlap of two peaks centered at slightly different distances (1.8 and 2.2 Å) from the Cr^{3+} ions, corresponding to water molecules in slightly different environments, namely, hydrogen bonded to

https://doi.org/10.1021/acs.jpcc.3c03901
J. Phys. Chem. C XXXX, XXX, XXX−XXX

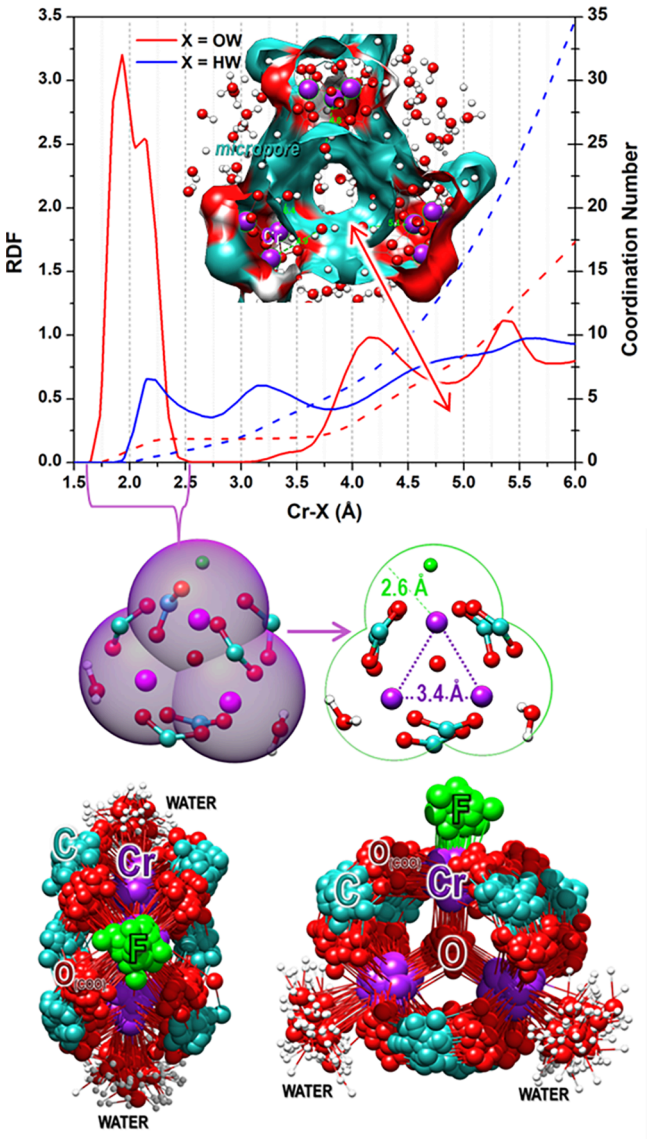

Figure 2. Top: Radial distribution functions of Cr^{3+} ions with water oxygens (OW) and hydrogens (HW). An example of a micropore, extracted from the last sampled configuration, filled with water molecules is shown in the inset. The water molecules belong to the second/third Cr shell. The Cr trimers at the vertices of the cavity structure do not contribute to the cavity walls, and a small contribution to the pore surface could be due to the oxygens connected to Cr. Middle: Typical arrangement of the three Cr^{3+} ions, six carboxylate moieties, and water molecules in the first shell. Bottom: The dynamics of the atoms are rendered by superimposed snapshots. Color codes: Cr, violet/magenta; C, dark cyan; O, red; H, white; F, green.

the nearby O(COO) or interacting with the outer water molecules through their hydrogen atoms. The structured water around Cr^{3+} is also confirmed by the Cr−HW RDF (Figure 2, top) peaks centered at 2.1 and 3.1 Å. It can be noticed that the position of the first peak is practically overlapped with the peak at 2.2 Å in the Cr−OW RDF plot, suggesting that the hydrogen atoms of a water molecule bound to Cr^{3+} are located at different distances from the metal center and that the peak at about 3.1 Å is due to the second hydrogen atom of the water molecule belonging to the first shell. Furthermore, the RDF intensity between the two peaks indicates hydrogen exchange.

Indeed, the inspection of the typical arrangement of the three Cr^{3+} ions, six carboxyl moieties, one fluorine atom (bound to one of the three Cr^{3+} ions), and two water molecules (each located in the first shell of the remaining Cr^{3+} ions), depicted in Figure 2 (middle), suggests a limited reorganization during the dynamics, which is dominated by the motion of the water hydrogens. The representative arrangement shown at the bottom of Figure 2 has been obtained by superimposing fifty configurations of one of the inorganic units of the MOF sampled during the final 100 ps of the MD trajectory. The evolution of the Cr−OW distance shown in Figure 3 confirms the stability of the water adsorption, and the short Cr−OW separation (first peak of the Cr−OW RDF in Figure 2) hints at water's propensity to become an OH species. The persistent presence of two water molecules in the trimer supports the view of a tight bond to Cr^{3+} reinforced by hydrogen bonding to the nearby O(COO)s.

Although the Cr trimers are at the borders of the micropores (where the organic linkers define the surface; see the inset in Figure 2 or Figure S10 for a clearer view), their distance from the water molecules is relatively long (4.8−5.4 Å). By examining the water content of all 130 micropores identified by the CAVER software (Figure 2 top) in the sampled configurations during the dynamics, we found that the number of water molecules inside each micropore was between five and eight (six on average, Figure S11), corresponding to about 4% of the total water amount (18300 molecules).

For the mesopores, an example of possible water filling is displayed in Figure S12. There, the combinations of spheres identifying the different pores are clipped to reveal the water content, which could be, as a consequence, partially undisplayed and thus underestimated. To disclose the organization of water in the mesopores, we calculated the RDF of all the water molecules in the model, of the water molecules within 3 Å of the carbon atoms (thus, near the walls of the pores), and of the water molecules within 3 Å of the Cr^{3+} ions (Figure S13). The trend of the distributions revealed that the only "structured" water molecules were those connected to the CUS. In contrast, the other water molecules behaved as bulk water, even though there was slight condensation on the pore walls. Another confirmation of this scenario comes from the spatial distribution function shown in Figure S14 where the yellow areas represent the various degrees of occupancy persistence of water. An evaluation of the migration ability of the water molecules in the mesopores suggests that, in 100 ps, a water molecule located in the second shell can migrate 1 nm from a Cr^{3+} ion (Figure S15).

3.2. Water in the Mesopores of MIL-101(Cr) by ^{1}H MAS NMR. To investigate water in the pores of MIL-101(Cr), ^{1}H MAS NMR spectra were recorded on dry MIL-101(Cr) and MIL-101(Cr)-45w, obtained by exposing the dry powder to a humid atmosphere. The ^{1}H MAS spectrum of dry MIL-101(Cr) shows the presence of four ^{1}H signals with isotropic chemical shifts of 2.6, 5.0, 7.9, and 14.3 ppm, as highlighted by the spectral deconvolution of the central band (Figure S4). The signals at 5.0 and 14.3 ppm were ascribed to the residual water and hydrogen atoms in the carboxylic groups of unreacted terephthalic acid trapped in the MOF's pores. In Figures 4a and S5, the ^{1}H MAS NMR spectrum recorded at a MAS rate of 20 kHz is shown, which is dominated by an anisotropic hyperfine shift due to the presence of the paramagnetic Cr^{3+} ions. From the analysis of the patterns of spinning side bands, the signals centered at 7.9 and 2.6 ppm

https://doi.org/10.1021/acs.jpcc.3c03901
J. Phys. Chem. C XXXX, XXX, XXX−XXX

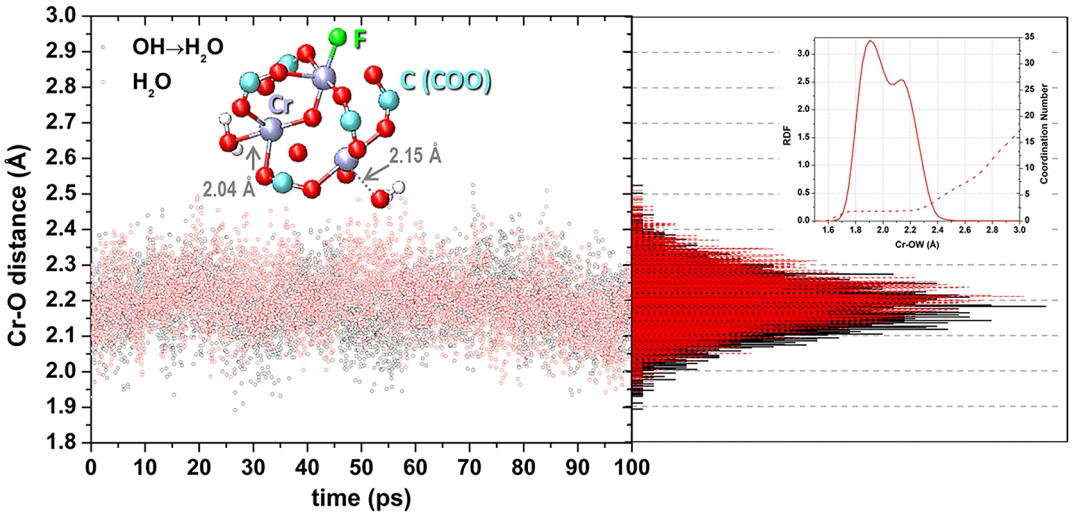

Figure 3. Left: Cr-OW vs time (last 100 ps of the MD trajectory) for a representative inorganic unit (inset) of the MOF. Right: distance distributions (corresponding RDF in the inset). Color codes: Cr, violet; C, dark cyan; O, red; H, white; F, green.

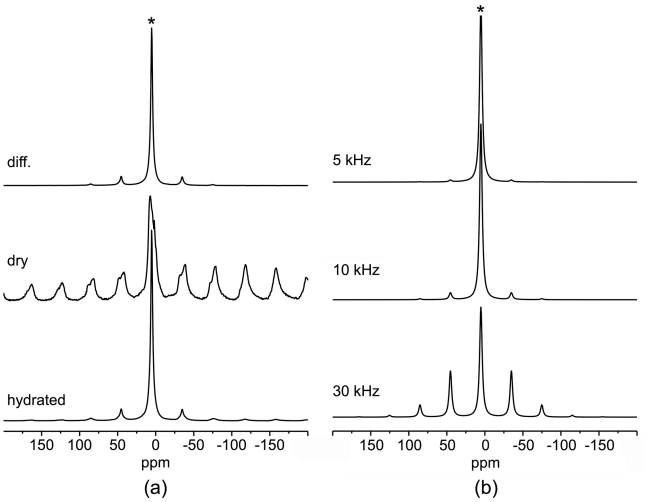

Figure 4. (a) ^{1}H MAS NMR spectra of dry MIL-101(Cr) and MIL-101(Cr)-45w recorded at a MAS rate of 20 kHz. The difference between the previous spectra is shown in the top trace. (b) Simulated ^{1}H MAS spectra of confined water subjected to residual dipolar interactions of 30 (bottom), 10 (middle), and 5 (top) kHz.

show different anisotropic hyperfine shift interactions. The pattern centered at 7.9 ppm is characterized by an anisotropic hyperfine shift interaction on the order of 30 ppm, as indicated by the occurrence of a maximum of only three side bands on each side of the central peak. For the signal centered at 2.6 ppm, ten side bands on each side are observed and the anisotropic hyperfine shift interaction is approximately 300 ppm. The pattern centered at 7.9 ppm is likely due to the aromatic protons of terephthalic acid trapped in the MOF's pores, while that centered at 2.6 ppm can be ascribed to the aromatic protons of the organic linkers of the framework. In fact, for the latter signal, the values of the isotropic chemical shift and of the anisotropic hyperfine shift compare well with those reported in ref 15 and there attributed to MIL-101(Cr) aromatic protons. Based on the signal observed in a similar compound, i.e., the trinuclear oxo-centered chromium carboxylate assembly $Cr_3O(O_2CMe)_6(D_2O)_3^+$,[21,41] the protons of water molecules located in the CUSs are expected to resonate at about 180 ppm. However, in our sample, no signal is observed in this region. This finding may be due to the signal broadening beyond the detection limit because of the paramagnetic interaction with the Cr^{3+} metal centers and/or the low amount of water molecules located in the CUSs.

Figure 4 shows the ^{1}H MAS NMR spectra of dry MIL-101(Cr) and hydrated MIL-101(Cr)-45w recorded with a spinning rate of 20 kHz together with their difference, corresponding to the signal of water. It is worth noticing that the porous space of MIL-101(Cr)-45w is almost entirely filled by water. Indeed, from the water vapor adsorption isobar, the maximum water uptake of MIL-101(Cr) is 55 wt % (Figure S2). Water located in micropores is most probably not detectable because it is present in low amounts in this kind of pore, as discussed in Section 3.1. Therefore, the difference signal is ascribable to water in the mesopores of MIL-101(Cr)-45w. The signal is centered at 5 ppm and exhibits first-order sidebands of low but appreciable intensity, symmetric with respect to the central band. The value of the isotropic chemical shift is close to that of bulk water. It must be pointed out that even if water molecules bonded to CUSs are not detectable *directly*, as indicated by the absence of the signal at 180 ppm, they might be detected *indirectly* because of the exchange between CUS water molecules and water molecules residing farther away from the surface. Indeed, the exchange would induce a shift of the position of the signal from the bulk value if the lifetime of water molecules located in CUSs is much shorter than the inverse of the difference of the resonance frequencies associated with water molecules in the two exchanging environments, i.e., ~2 μs, and the population of each site is not negligible. Therefore, since we do not observe a significant shift of the position of the signal from the bulk value, the lifetime of CUS water molecules is longer than 2 μs and/or the population of water in CUSs is negligible. This issue will be addressed again in Section 3.4. The sidebands exhibited by the 5 ppm signal come from the residual dipolar interaction between the two hydrogen atoms of the water molecules. By comparing the experimental spectrum with spectra simulated in the presence of dipolar interactions with different strengths (dipolar coupling constants of 5, 10, and 30 kHz, the latter value corresponding to that of a rigid water molecule), shown in Figure 4b, we estimated a ^{1}H-^{1}H residual

https://doi.org/10.1021/acs.jpcc.3c03901
J. Phys. Chem. C XXXX, XXX, XXX−XXX

dipolar coupling of approximately 10 kHz. Considering the arrangement of water in the mesopores as derived from MD simulations (Figure S13), we can infer that the observed reduction of the dipolar coupling arises from a fast exchange between structured water close to the pore surface and "bulk" water located in the inner part of the pore.[42]

3.3. Water Distribution in Intra- and Intergrain Spaces of MIL-101(Cr) by Low-Field ^{1}H T_2 and T_1 Measurements. ^{1}H CPMG curves were recorded on the MIL-101(Cr)-Xw samples with different amounts of water ranging between 45 and 90 wt %. MIL-101(Cr)-45w was prepared by exposing dry MIL-101(Cr) to a humid atmosphere. As previously discussed, in this sample, the intragrain space is almost entirely filled by water. The other samples were prepared by imbibition of the dry powder with amounts of water ranging between 68 and 90 wt %. The decays, exemplified in Figure 5, exhibit a biexponential behavior for all the samples except MIL-101(Cr)-45w, which shows a monoexponential behavior with a decay constant, T_{2a}, of 2 ms. The fast decaying component of the biexponential curves of the imbibed samples is characterized by a decay time T_{2a} of about 3.5 ms. In contrast, the long decaying component displays a decay time T_{2b} increasing from 57 to 270 ms with increasing amount of water. The fitting curves, together with their components, are shown in the figure, and the corresponding fitting parameters (i.e., relaxation time values and weight fractions) are displayed in Table 1. The trend of the weight of the long decaying component, w_{2b}, as a function of the water amount is shown in Figure 6a, while those of T_{2a} and T_{2b} are displayed in Figure 6b. As we can see, for the imbibed samples, w_{2b} linearly increases upon increasing the amount of water, and a value of $w_{2b} = 0$ corresponds to a water amount of 55 wt % as determined by linear extrapolation.

On the basis of these findings, the two T_2 components are ascribable to two distinct water populations, which do not undergo fast exchange with each other. The fast decaying component is due to water located in the intragrain mesopores of MIL-101(Cr), while the long decaying one arises from water in the larger intergrain spaces, which are progressively filled as the water amount increases. Water in the intragrain mesopores exhibits a much lower value of T_2 compared to intergrain water because surface effects are dominant. Interestingly, T_{2a} is independent of water amount for the imbibed samples (Table 1 and Figure 6b), indicating that the intragrain spaces of MIL-101(Cr) are completely filled at the investigated water loadings. The slight difference between the value of T_{2a} shown by the imbibed samples and the one exhibited by MIL-101(Cr)-45w is attributable to an incomplete filling of the intragrain spaces due to the fact that we are below 55 wt % of water, as well as to the possible presence of water molecules also on the external surface of the grains. On the other hand, T_{2b} increases by increasing the water loading, reflecting that water progressively fills the intergrain space, and its relaxation, resulting from the fast exchange of water molecules between the grain surface and the bulk, is less and less affected by surface effects. It must be noted that the long decaying component becomes detectable above a water amount threshold of about 55 wt %, which corresponds to the amount of water necessary to fill the intragrain spaces according to the water adsorption isobar (Figure S2). Analogous results were previously obtained for solvent-imbibed MOFs characterized by different intra- and intergrain space sizes.[43]

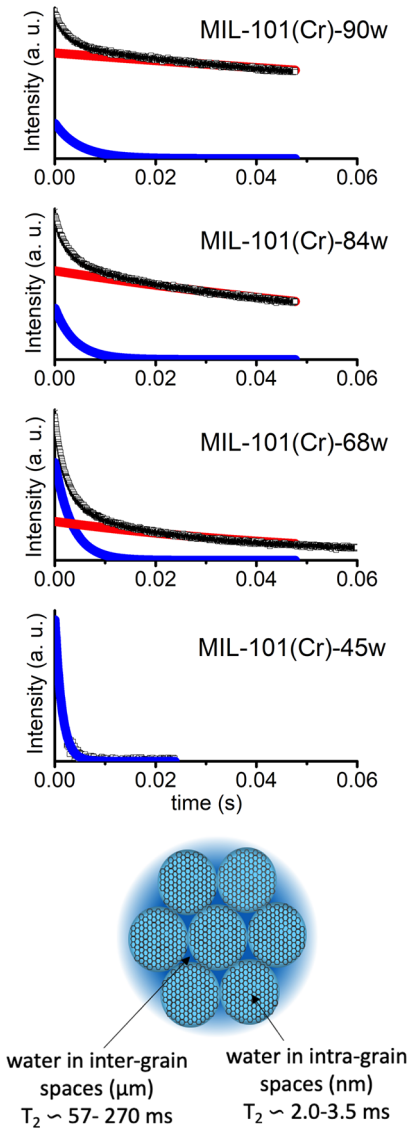

Figure 5. ^{1}H CPMG curves (black dots) of the indicated MIL-101(Cr)-Xw samples. For each sample, the best fitting biexponential function (black line) used to fit the experimental decay together with the short (blue line) and long (red line) T_2 components are shown. On the bottom, packed porous crystals containing water in the inter- and intragrain spaces are schematically represented and the length scales of the two environments are reported. The intergrain spaces are estimated on the basis of the crystal size, which was derived from SEM images (see Figure S3).

The ^{1}H longitudinal relaxation of water was also investigated at 21 MHz on the same samples. For all the imbibed samples, the longitudinal magnetization recovery is biexponential, whereas it is monoexponential for MIL-101(Cr)-45w. The best-fitting values for the short and long relaxation times (T_{1a} and T_{1b}, respectively) are shown in Table 1, whereas their trends as a function of the water amount are displayed in Figure 6b. T_{1a} values are on the order of a few milliseconds at all water loadings, whereas T_{1b} increases with the water amount. As for T_2, these two T_1 components are ascribable to the two water populations in the intra- (T_{1a}) and intergrain (T_{1b}) spaces. Indeed, the values of both T_{1a} and T_{1b} are similar to those of T_{2a} and T_{2b}, respectively, and the weight of each T_1 component is close to the corresponding value of the T_2 one.

https://doi.org/10.1021/acs.jpcc.3c03901
J. Phys. Chem. C XXXX, XXX, XXX−XXX

Table 1. ^{1}H T_2 and T_1 Components (T_{2i} and T_{1i}, in ms) and Corresponding Weight Fractions (w_{2i} and w_{1i}) Determined for the Indicated MIL-101(Cr)-Xw Samples at 25 °C[a]

Sample	T_{2a} (w_{2a})	T_{2b} (w_{2b})	T_{1a} (w_{1a})	T_{1b} (w_{1b})
MIL-101(Cr)-90w	3.5 (0.25)	270 (0.75)	6 (0.1)	430 (0.9)
MIL-101(Cr)-88w	3.5 (0.30)	130 (0.70)	6 (0.2)	221 (0.8)
MIL-101(Cr)-84w	3.5 (0.35)	113 (0.65)	6 (0.3)	190 (0.7)
MIL-101(Cr)-77w	3.5 (0.55)	95 (0.45)	4 (0.5)	107 (0.5)
MIL-101(Cr)-68w	3.5 (0.70)	57 (0.30)	4 (0.7)	54 (0.3)
MIL-101(Cr)-45w	2.0 (1.0)		2.0 (1.0)	

[a]Index $i = a$ and b denotes fast and long decaying components, respectively. Errors on relaxation times and weight fractions are of 1 unit on the last digit.

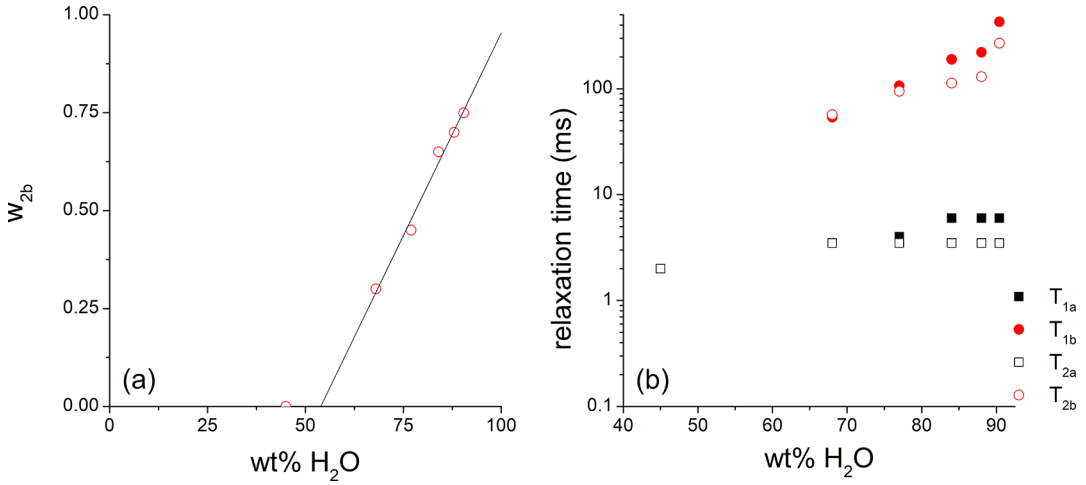

Figure 6. (a) Plot of w_{2b} of the MIL-101(Cr)-Xw samples vs the weight percentage of water (wt %). (b) Trends of T_{2a}, T_{2b}, T_{1a}, and T_{1b} at 21 MHz and 25 °C obtained for the same samples as a function of water wt %.

The slight discrepancies between the weight values determined from T_1 and T_2 analyses are due to experimental error, which is higher for T_1 data because of less dense data sampling at short recovery times.

Further support to this scenario, where the water populations of the two distinct compartments do not undergo fast exchange between each other, is provided considering that the diffusion length walked by a water molecule during relaxation is only 10−100 times larger than the size of each compartment. Indeed, the diffusion length is 5−10 μm for the intragrain water (size of a grain ∼ 0.5 μm) and 30−80 μm for the intergrain water (intergrain space ≈ 1 μm), assuming that water diffuses isotropically with a diffusion coefficient equal to that of bulk water. Since the trajectory of a water molecule is convoluted, it is likely to remain confined within a compartment, thus hinting that exchange does not occur during time for relaxation.

3.4. Residence Time of Water on MIL-101(Cr) Open Sites by ^{1}H FFC NMR Relaxometry. To gain insight into the details of the interaction of water with chromium sites, which is at the basis of relaxation enhancement of water protons, ^{1}H NMRD curves (i.e., $R_1 = 1/T_1$ vs ^{1}H Larmor frequency) were recorded on MIL-101(Cr)-90w using FFC NMR relaxometry. For this sample, a monoexponential longitudinal relaxation decay characterized by a T_1 of 300 ms was observed at 25 °C at the frequency of 21 MHz, ascribable to water in the intergrain spaces. The short decaying component ascribed to water in the mesopores, which at this loading level should account for only 10% of protons, was filtered off in this measurement by sampling the signal recovery at delay times longer than T_{1a} (6 ms; see Table 1). Since T_1 tends to decrease upon decreasing the frequency, the filter is supposed to be effective also at frequencies smaller than 21 MHz. The sample at the highest water loading was chosen because, for lower amounts of water, the shortening of T_1 of intergrain water and the decrease of its weight prevent the acquisition of FFC data with a suitable signal-to-noise ratio. On the other hand, the sample containing solely water within the intragrain spaces, MIL-101(Cr)-45w, exhibited a T_1 value of only 2 ms at 21 MHz, as determined with the fixed field spectrometer (see Table 1) and confirmed by a measurement conducted using the FFC NMR relaxometer at 21 MHz. Since T_1 tends to decrease upon decreasing the Larmor frequency, T_1 values at frequencies lower than 21 MHz were expected to be too short to be accurately measured with the FFC NMR technique. The ^{1}H R_1 NMRD curves of MIL-101(Cr)-90w acquired at 25, 55 and 70 °C are shown in Figure 7. The curve recorded at 25 °C shows a dispersion centered at about 9 MHz. In the region between 0.1 and 1 MHz, R_1 does not show any significant frequency dependence, whereas at frequencies smaller than 0.1 MHz, a small but appreciable increase is detectable. At high frequencies, the data show a slight curvature, hinting that a plateau of R_1 is being reached. The R_1 value at the plateau is about 3 s^{-1}, much larger than that characterizing bulk water, for which we measured a R_1 value of only 0.3 s^{-1} at 21 MHz. Therefore, the observed large plateau value is mainly ascribable to the contribution from the surface relaxation term, $\frac{N_{surf}}{N}\frac{1}{T_{1surf}}$, introduced in section 2.3.4.

The dispersion centered at about 9 MHz tends to shift to higher frequencies with an increase in the temperature.

https://doi.org/10.1021/acs.jpcc.3c03901
J. Phys. Chem. C XXXX, XXX, XXX−XXX

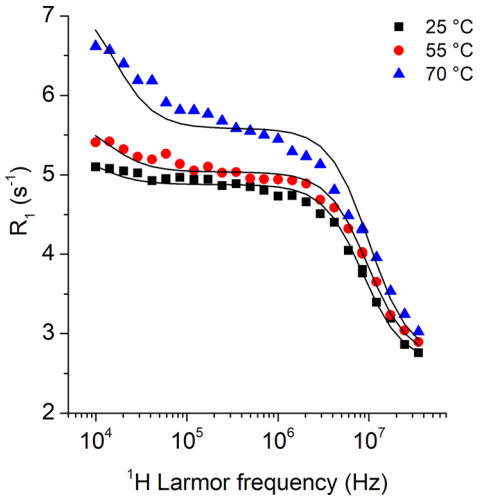

Figure 7. ^{1}H R_1 NMRD curves (symbols) at the indicated temperatures of MIL-101(Cr)-90w. For each temperature, the best fit curves (solid lines) obtained as described in the main text are also shown.

Moreover, the increase of R_1 at frequencies below 0.1 MHz becomes more pronounced at high temperature, and the tail of a R_1 dispersion is visible in the curve recorded at 70 °C. In the whole frequency range, R_1 increases upon heating, and this trend is indicative of a thermally activated exchange process.

The observed NMRD curves are ascribed to paramagnetic relaxation induced by modulation of the dipolar interactions between the CUS water protons and the Cr^{3+} unpaired electrons. According to eq 3, the dispersion centered at about 9 MHz corresponds to a correlation time equal to ω_H^{-1}, which falls in the 20−30 ns range. The low-frequency dispersion associated with these interactions is expected to be centered on the very low side of the available spectral range, at a frequency (corresponding to ω_S in eq 3) of about 9 MHz/658 = 0.014 MHz, with 658 being the absolute value of the ratio between the electron and proton magnetogyric ratios. The R_1 increase at frequencies smaller than 0.1 MHz is ascribed to this low-field dispersion. The fact that the low-field dispersion is very modest in the low-temperature profile can be explained by a slow exchange between water molecules directly bound to Cr^{3+} ions and nearby water molecules. In particular, below 70 °C, τ_M is expected to be much longer than T_{1Cr} at low fields, which would hinder an increase of the relaxation rate (eq 2), so that the low field dispersion is not observed.

To extract quantitative parameters from the NMRD curves, we employed the equations presented in section 2.3.4 to fit the data. The experimental features of the R_1 NMRD curves are caught by expressing the relaxation rate of the bound water, $\frac{1}{T_{1Cr}}$, using the most probable Cr-HW distances found by MD simulations and simply changing the lifetime τ_M. In particular, $\frac{1}{T_{1Cr}}$ is expressed as the sum of a contribution from a hydrogen atom characterized by a r_{CrH1} of 2.2 Å $\left(\frac{1}{T_{1Cr1}}\right)$ and another one characterized by a r_{CrH2} of 3.1 Å $\left(\frac{1}{T_{1Cr2}}\right)$ according to the following equation:

$$\frac{1}{T_{1Cr}} = \frac{1}{2}\frac{1}{T_{1Cr1}} + \frac{1}{2}\frac{1}{T_{1Cr2}} \quad (7)$$

$\frac{1}{T_{1Cr1}}$ is about 1 order of magnitude larger than $\frac{1}{T_{1Cr2}}$ and dominates relaxation. The electronic relaxation times T_{1e} and T_{2e} do not affect the calculated trends, because they exhibit values much larger than τ_M. Therefore, in the assumed model (eqs 3−7), the parameters to be optimized in the NMRD curve analyses are the sum $\frac{N_{surf}}{N}\frac{1}{T_{1surf}} + \frac{N_{bulk}}{N}\frac{1}{T_{1bulk}}$, $\frac{N_{param}}{N}$, and τ_M, only the latter being dependent on temperature. We assumed that the sum $\frac{N_{surf}}{N}\frac{1}{T_{1surf}} + \frac{N_{bulk}}{N}\frac{1}{T_{1bulk}}$ adds a contribution independent of frequency, which is referred to as *plateau value* in Table 2, which was found to be 2.7 s^{-1} in all cases. τ_M values of tens of ns were determined from the fittings, tending to decrease upon heating, whereas the parameter $\frac{N_{param}}{N}$ resulted to be 1.3×10^{-7}. The best-fit parameters are reported in Table 2, and the fitting curves are displayed in Figure 7. As can be observed, the main features of the NMRD curves are satisfactorily reproduced at all temperatures.

Table 2. Best Fit Parameters Obtained by Fitting the R_1 NMRD Curves of MIL-101(Cr)-90w at the Indicated Temperatures Using the Model Described in Section 3

Parameters				
Independent of temperature	Dependent on temperature	25 °C	55 °C	70 °C
$N_{param}/N = 1.3 \times 10^{-7}$	τ_M (ns)	51	48	22
plateau value = 2.7 s^{-1}				

It must be observed that the contribution to R_1 from a water molecule located in the second shell is negligible if, for this type of water molecule, we suppose r_{CrH} distances ranging between 3.2 and 4.8 Å and a lifetime of 100 ps or shorter on the basis of our MD simulations. Moreover, the possible contribution to relaxation from the Fermi contact interaction of a bound water molecule with the unpaired electrons on Cr^{3+} was also found to be negligible compared to that arising from the dipolar interaction (data not shown), considering an estimation performed by fixing the contact coupling constant to the value reported for the Cr^{3+} aqua ion (2 MHz)[40] and using the parameters displayed in Table 2. The equations used to evaluate the contribution to R_1 from a water molecule in the second shell and from the Fermi contact interaction are shown in Section S4 of the Supporting Information.

The extracted τ_M values are likely "average" values of the water exchange rate. It is reasonable to suppose that different sites having different exchange rates are present in the MOF. Moreover, the τ_M values are much shorter than 2 μs, the limit value introduced in Section 3.2, where we stated that a lifetime longer than 2 μs or a negligible population of water in CUSs would be compatible with the ^{1}H chemical shift data determined from ^{1}H MAS NMR spectra. Therefore, since the values of τ_M determined by FFC NMR are not longer than 2 μs, we should conclude that the population of water in CUSs is negligible.

Interestingly, the τ_M values here determined for Cr^{3+} ions on the MOF surface are 2 orders of magnitude shorter than those found for $Cr(H_2O)_6^{3+}$ ions in water,[40] suggesting a different mechanism for water exchange between the first and the second coordination shell, possibly associated to the different coordination of Cr^{3+} in the aqua ion and in the MOF CUS. Indeed, for complexes in water, it is known that substituting

https://doi.org/10.1021/acs.jpcc.3c03901
J. Phys. Chem. C XXXX, XXX, XXX−XXX

some of the first shell water molecules of an aqua ion with one or more kinetically inert ligands can have a strong influence on the rate and on the exchange mechanism of the remaining water molecule(s).[17]

It is interesting to compare the value of $\frac{N_{param}}{N}$ obtained from the fitting with that derived using other data available to us. In particular, we evaluated the ratio by assessing N_{param} and N separately, exploiting structural parameters, i.e., the grain size from SEM images (Figure S3), the average surface occupied by a trimer made of three chromium atoms, as derived from RDF of the Cr ions (Figure S7), the density of MIL-101(Cr), taken from ref 27, and the relative amount of water and powder. The details of the calculations are reported in Section S3 of the Supporting Information. We found that $\frac{N_{param}}{N} \approx 10^{-4}$. Although this estimate is based on rough approximations, the discrepancy with the value determined from the analysis of the FFC NMR data is very large and is likely due to a poor accessibility of water to CUSs, possibly related to grain agglomeration and/or to surface defects.

4. CONCLUSIONS

We investigated the state of water in MIL-101(Cr) by combining ^{1}H MAS NMR, NMR relaxometry, and classical reactive MD simulations. Although the MD simulations clearly showed that water molecules are coordinated to the open metal sites of the MOF, no experimental evidence proving the coordination was gained with ^{1}H MAS NMR because of the low population of the sites and the line broadening of the water proton signal due to the closeness of water to the paramagnetic Cr^{3+} ion. On the other hand, through the detection of ^{1}H−^{1}H residual dipolar interaction, ^{1}H MAS NMR did reveal the presence of structured water close to the mesopore surface (but not bound to Cr), in agreement with the MD simulations. This type of water undergoes fast exchange with "bulk" water located in the inner part of the pores.

Experimental evidence of water bound to the open metal sites was instead obtained by applying ^{1}H FFC NMR relaxometry, where distinctive features in the NMRD dispersion profiles pointed to the presence of this type of water. Since this technique could not accurately detect water in the intragrain mesopores due to the short relaxation times of water protons, we selectively probed water molecules located in the intergrain spaces of the MOF. The NMRD dispersion curves were interpreted within a model which is generally applied to water binding to paramagnetic ions in solution. Here, the model was extended to the case of Cr^{3+} paramagnetic ions fixed on the MOF surface. Within the model, exchange of a water molecule between the first and the second shell of a Cr^{3+} ion occurs, and lifetimes in the first shell of tens of nanoseconds were assessed. This result is quite noticeable because only a few experimental techniques allow solvent lifetimes to be measured directly. Interestingly, the measured lifetimes are 2 orders of magnitude shorter that those found in the aqua Cr^{3+} complex in solution, suggesting that the mechanism of water exchange in MIL-101(Cr) is different from that in the aqua ion. This evidence raises questions about the factors that influence the mechanism of exchange, which are beyond the scope of the present study but certainly deserve further attention. Moreover, the ^{1}H FFC NMR data provided information on the accessibility of the open metal sites located on the grain external surface, revealing that only a small fraction of the sites are accessible, and this has implications for the grain agglomeration and surface defects.

■ ASSOCIATED CONTENT

Supporting Information

The Supporting Information is available free of charge at https://pubs.acs.org/doi/10.1021/acs.jpcc.3c03901.

Materials and Methods: X-Ray diffraction pattern of MIL-101(Cr); Nitrogen adsorption data of MIL-101(Cr); Water vapor adsorption isobar of MIL-101(Cr) recorded at the water vapor pressure of 2.5 kPa; SEM image of MIL-101(Cr); Central band of ^{1}H MAS NMR spectrum of dry MIL-101(Cr) recorded with a spinning rate of 67 kHz; ^{1}H MAS NMR spectrum of dry MIL-101(Cr) recorded at a spinning rate of 20 kHz. MD Simulations: Snapshot of solvated MOF model; Atom−atom RDF of Cr^{3+} ions compared with RDF of crystallographic structure; Atom−atom RDF of carboxyl oxygens with Cr^{3+} ions and with water hydrogens; Lifetime distribution of water molecules within 4.85 Å (comprising the first and the second coordination layer) of Cr atoms during the last 100 ps of MD trajectory (total simulation time: 500 ps); Snapshot extracted from MD simulations showing a representative portion of a micropore filled with water; Snapshot extracted from MD simulations, disclosing the water content in some micropores; Snapshot extracted from MD simulations, disclosing all water molecules diffusing in the model and inside some mesopores; Atom−atom radial distribution functions of water (OW−OW) inside the MOF; Spatial distribution functions of water molecules; Migration of a water molecule from the second shell to the outer region. Calculation of $\frac{N_{param}}{N}$ using structural information. Evaluation of contributions to R_1 from second shell water molecules and from contact coupling (PDF)

■ AUTHOR INFORMATION

Corresponding Author

Silvia Pizzanelli − *Centro per l'Integrazione della Strumentazione Scientifica dell'Università di Pisa (CISUP), 56126 Pisa, Italy; Istituto di Chimica dei Composti OrganoMetallici, Consiglio Nazionale delle Ricerche—CNR, 56124 Pisa, Italy;* orcid.org/0000-0002-1150-1551; Phone: +39 0503152549; Email: silvia.pizzanelli@pi.iccom.cnr.it

Authors

Francesca Martini − *Dipartimento di Chimica e Chimica Industriale, Università di Pisa, 56124 Pisa, Italy; Centro per l'Integrazione della Strumentazione Scientifica dell'Università di Pisa (CISUP), 56126 Pisa, Italy; Istituto di Chimica dei Composti OrganoMetallici, Consiglio Nazionale delle Ricerche—CNR, 56124 Pisa, Italy*

Lucia Calucci − *Centro per l'Integrazione della Strumentazione Scientifica dell'Università di Pisa (CISUP), 56126 Pisa, Italy; Istituto di Chimica dei Composti OrganoMetallici, Consiglio Nazionale delle Ricerche—CNR, 56124 Pisa, Italy;* orcid.org/0000-0002-3080-8807

Larisa G. Gordeeva − *Boreskov Institute of Catalysis, Novosibirsk 630090, Russia;* orcid.org/0000-0001-8308-0111

https://doi.org/10.1021/acs.jpcc.3c03901
J. Phys. Chem. C XXXX, XXX, XXX−XXX

Susanna Monti − *Istituto di Chimica dei Composti OrganoMetallici, Consiglio Nazionale delle Ricerche—CNR, 56124 Pisa, Italy;* orcid.org/0000-0002-3419-7118
Marina V. Solovyeva − *Boreskov Institute of Catalysis, Novosibirsk 630090, Russia*
Cheherazade Trouki − *Istituto per i Processi Chimico-Fisici, Consiglio Nazionale delle Ricerche—CNR, 56124 Pisa, Italy; Dipartimento di Farmacia, Università di Pisa, 56126 Pisa, Italy;* orcid.org/0000-0002-1303-3595

Complete contact information is available at: https://pubs.acs.org/10.1021/acs.jpcc.3c03901

Notes

The authors declare no competing financial interest.

■ ACKNOWLEDGMENTS

This research was partially funded by the University of Pisa grant PRA_2022_34 "Optimizing intermolecular interactions for recognition catalysis and green chemistry". The authors would like to thank Dr. Claudia Forte and Dr. Angelo Freni for many helpful discussions.

■ REFERENCES

(1) Khan, N. A.; Hasan, Z.; Jhung, S. H. Adsorptive Removal of Hazardous Materials Using Metal-Organic Frameworks (MOFs): a Review. *J. Hazard. Mater.* **2013**, *244-245*, 444−456.
(2) Pascanu, V.; Miera, G. G.; Inge, A. K.; Martín-Matute, B. Metal-Organic Frameworks as Catalysts for Organic Synthesis: a Critical Perspective. *J. Am. Chem. Soc.* **2019**, *141*, 7223−7234.
(3) Wu, Z.; Li, Y.; Zhang, C.; Huang, X.; Peng, B.; Wang, G. Recent Advances in Metal-Organic Framework-Based Catalysts for Thermocatalytic Selective Oxidation of Organic Substances. *Chem Catal.* **2022**, *2*, 1009−1045.
(4) Bavykina, A.; Kolobov, N.; Khan, I.; Bau, J. A.; Ramirez, A.; Gascon, J. Metal-Organic Frameworks in Heterogeneous Catalysis: Recent Progress, New Trends, and Future Perspectives. *Chem. Rev.* **2020**, *120*, 8468−8535.
(5) Zorainy, M. Y.; Gar Alalm, M.; Kaliaguine, S.; Boffito, D. C. Revisiting the MIL-101 Metal-Organic Framework: Design, Synthesis, Modifications, Advances, and Recent Applications. *J. Mater. Chem. A* **2021**, *9*, 22159−22217.
(6) Maes, M.; Trekels, M.; Boulhout, M.; Schouteden, S.; Vermoortele, F.; Alaerts, L.; Heurtaux, D.; Seo, Y.; Hwang, Y. K.; Chang, J.; Beurroies, I.; et al. Selective Removal of N-Heterocyclic Aromatic Contaminants from Fuels by Lewis Acidic Metal−Organic Frameworks. *Angew. Chem.* **2011**, *123*, 4296.
(7) Nuzhdin, A. L.; Kovalenko, K. A.; Dybtsev, N.; Bukhtiyarova, G. A. Removal of Nitrogen Compounds from Liquid Hydrocarbon Streams by Selective Sorption on Metal-Organic Framework MIL-101. *Mendeleev Commun.* **2010**, *20*, 57−58.
(8) Ahmed, I.; Khan, N. A.; Hasan, Z.; Jhung, S. H. Adsorptive Denitrogenation of Model Fuels with Porous Metal-Organic Framework (MOF) MIL-101 Impregnated with Phosphotungstic Acid: Effect of Acid Site Inclusion. *J. Hazard. Mater.* **2013**, *250−251*, 37−44.
(9) Seo, P. W.; Ahmed, I.; Jhung, S. H. Adsorption of Indole and Quinoline from a Model Fuel on Functionalized MIL-101: Effects of H-bonding and Coordination. *Phys. Chem. Chem. Phys.* **2016**, *18*, 14787−14794.
(10) Mao, Y.; Qi, H.; Ye, G.; Han, L.; Zhou, W.; Xu, W.; Sun, Y. Green and Time-Saving Synthesis of MIL-100(Cr) and its Catalytic Performance. *Microporous Mesoporous Mater.* **2019**, *274*, 70−75.
(11) Rivera-Torrente, M.; Pletcher, P. D.; Jongkind, M. K.; Nikolopoulos, N.; Weckhuysen, B. M. Ethylene Polymerization over Metal-Organic Framework Crystallites and the Influence of Linkers on Their Fracturing Process. *ACS Catal.* **2019**, *9*, 3059−3069.
(12) Santiago-Portillo, A.; Navalón, S.; Concepción, P.; Álvaro, M.; García, H. Influence of Terephthalic Acid Substituents on the Catalytic Activity of MIL-101(Cr) in Three Lewis Acid Catalyzed Reactions. *ChemCatChem* **2017**, *9*, 2506−2511.
(13) Zhao, T.; Dong, M.; Yang, L.; Liu, Y. Synthesis of Stable Hierarchical MIL-101(Cr) with Enhanced Catalytic Activity in the Oxidation of Indene. *Catalysts* **2018**, *8*, 394.
(14) Aguila, B.; Sun, Q.; Wang, X.; O'Rourke, E.; Al-Enizi, A. M.; Nafady, A.; Ma, S. Lower Activation Energy for Catalytic Reactions through Host−Guest Cooperation within Metal−Organic Frameworks. *Angew. Chem., Int. Ed.* **2018**, *57*, 10107−10111.
(15) Wittmann, T.; Mondal, A.; Tschense, C. B. L.; Wittmann, J. J.; Klimm, O.; Siegel, R.; Corzilius, B.; Weber, B.; Kaupp, M.; Senker, J. Probing Interactions of N-Donor Molecules with Open Metal Sites within Paramagnetic Cr-MIL-101: A Solid-State NMR Spectroscopic and Density Functional Theory Study. *J. Am. Chem. Soc.* **2018**, *140*, 2135−2144.
(16) Khudozhitkov, A. E.; Arzumanov, S. S.; Kolokolov, D. I.; Kholdeeva, O. A.; Freude, D.; Stepanov, A. G. Guests Like Gear Levers: Donor Binding to Coordinatively Unsaturated Metal Sites in MIL-101 Controls the Linker's Rotation. *Chem. Eur. J.* **2019**, *25*, 5163−5168.
(17) Helm, L.; Merbach, A. E. Inorganic and Bioinorganic Solvent Exchange Mechanisms. *Chem. Rev.* **2005**, *105*, 1923−1959.
(18) Khudozhitkov, A. E.; Toktarev, A. V.; Arzumanov, S. S.; Gabrienko, A. A.; Kolokolov, D. I.; Stepanov, A. G. ^{2}H Solid-State NMR Spectroscopy Reveals the Dynamics of a Pyridine Probe Interacting with Coordinatively Unsaturated Metal Sites of MIL-100(Al) Metal−Organic Frameworks. *Chem. Eur. J.* **2019**, *25*, 10808−10812.
(19) Gao, J.; Fei, S.; Ho, Y.-L.; Matsuda, R.; Daiguji, H.; Delaunay, J.-J. Water Confined in MIL-101(Cr): Unique Sorption−Desorption Behaviors Revealed by Diffuse Reflectance Infrared Spectroscopy and Molecular Dynamics Simulation. *J. Phys. Chem. C* **2021**, *125*, 17786−17795.
(20) Dubbeldam, D.; Calero, S.; Ellis, D. E.; Snurr, R. Q. RASPA: Molecular Simulation Software for Adsorption and Diffusion in Flexible Nanoporous Materials. *Mol. Simul.* **2016**, *42*, 81−101.
(21) Bertini, I.; Luchinat, C.; Parigi, G.; Ravera, E. *NMR of Paramagnetic Molecules. Applications to Metallobiomolecules and Models*, 2nd ed.; Elsevier: Amsterdam, 2017.
(22) Carné-Sánchez, A.; Bonnet, C. S.; Imaz, I.; Lorenzo, J.; Tóth, É.; Maspoch, D. Relaxometry Studies of a Highly Stable Nanoscale Metal−Organic Framework Made of Cu(II), Gd(III), and the Macrocyclic DOTP. *J. Am. Chem. Soc.* **2013**, *135*, 17711−17714.
(23) Pereira, G. A.; Peters, J. A.; Almeida Paz, F. A.; Rocha, J.; Geraldes, C. F. G. C. Evaluation of [Ln(H_2cmp)(H_2O)] Metal-Organic Framework Materials for Potential Application as Magnetic Resonance Imaging Contrast Agents. *Inorg. Chem.* **2010**, *49*, 2969−2974.
(24) Pizzanelli, S.; Freni, A.; Farmahini, A. H.; Gordeeva, L. G.; Sarkisov, L.; Solovyeva, M. V.; Forte, C. Water Dynamics in NH_2-MIL-125: Insights from a Combined ^{1}H NMR Relaxometry and Computational Investigation. *J. Phys. Chem. C* **2021**, *125*, 14416−14429.
(25) Solovyeva, M. V.; Gordeeva, L. G.; Aristov, Y. I. MIL-101(Cr)−Methanol as Working Pair for Adsorption Heat Transformation Cycles: Adsorbent Shaping, Adsorption Equilibrium and Dynamics. *Energy Convers. Manage.* **2019**, *182*, 299−306.
(26) Lebedev, O. I.; Millange, F.; Serre, C.; Van Tendeloo, G.; Férey, G. First Direct Imaging of Giant Pores of the Metal-Organic Framework MIL-101. *Chem. Mater.* **2005**, *17* (26), 6525−6527.
(27) Ferey, G.; Mellot-Draznieks, C.; Serre, C.; Millange, F.; Dutour, J.; Surble, S.; Margiolaki, I. A Chromium Terephthalate-Based Solid with Unusually Large Pore Volumes and Surface Area. *Science* **2005**, *309*, 2040−2042.
(28) Pizzanelli, S.; Monti, S.; Gordeeva, L. G.; Solovyeva, M. V.; Freni, A.; Forte, C. A Close View of the Organic Linker in a MOF: Structural Insights from a Combined ^{1}H NMR Relaxometry and

Computational Investigation. *Phys. Chem. Chem. Phys.* **2020**, *22*, 15222−15230.
(29) Baerends, E. J.; Ziegler, T.; Atkins, A. J.; Autschbach, J.; Baseggio, O.; Bashford, D.; Bérces, A.; Bickelhaupt, F. M.; Bo, C.; Boerrigter, P. M. et al. *ADF, adf2019.102*; SCM: Amsterdam, The Netherlands, 2019. http://www.scm.com (accessed 01 July, 2023).
(30) Meiboom, S.; Gill, D. Modified Spin-Echo Method for Measuring Nuclear Relaxation Times. *Rev. Sci. Instrum.* **1958**, *29*, 688−691.
(31) Korb, J.-P.; Hodges, M. W.; Gobron, T.; Bryant, R. G. Anomalous Surface Diffusion of Water Compared to Aprotic Liquids in Nanopores. *Phys. Rev. E* **1999**, *60*, 3097−3106.
(32) Korb, J. -P.; Freiman, G.; Nicot, B.; Ligneul, P. Dynamical Surface Affinity of Diphasic Liquids as a Probe of Wettability of Multimodal Porous Media. *Phys. Rev. E* **2009**, *80*, No. 061601.
(33) Korb, J. -P. Nuclear Magnetic Relaxation of Liquids in Porous Media. *New J. Phys.* **2011**, *13*, No. 035016.
(34) Korb, J. -P. Multiscale Nuclear Magnetic Relaxation Dispersion of Complex Liquids in Bulk and Confinement. *Prog. Nucl. Magn. Reson. Spectrosc.* **2018**, *104*, 12−55.
(35) Gizatullin, B.; Mattea, C.; Shikhov, I.; Arns, C.; Stapf, S. Modeling Molecular Interactions with Wetting and Non-Wetting Rock Surfaces by Combining Electron Paramagnetic Resonance and NMR Relaxometry. *Langmuir* **2022**, *38*, 11033−11053.
(36) Stapf, S.; Shiknov, I.; Arns, C.; Gizatullin, B.; Mattea, C. Dipolar NMR Relaxation of Adsorbates on Surfaces of Controlled Wettability. *Magn. Reson. Lett.* **2023**, DOI: 10.1016/j.mrl.2023.02.001.
(37) Gizatullin, B.; Mattea, C.; Stapf, S. Radicals on the Silica Surface: Probes for Studying Dynamics by Means of Fast Field Cycling Relaxometry and Dynamic Nuclear Polarization. *Magn. Reson. Lett.* **2023**, DOI: 10.1016/j.mrl.2023.03.006.
(38) Bloembergen, N.; Morgan, L. O. Proton Relaxation Times in Paramagnetic Solutions. Effects of Electron Spin Relaxation. *J. Chem. Phys.* **1961**, *34*, 842−850.
(39) Rubinstein, M.; Baram, A.; Luz, Z. Electronic and Nuclear Relaxation in Solutions of Transition Metal Ions with Spin S = 3/2 and 5/2. *Mol. Phys.* **1971**, *20*, 67−80.
(40) Bertini, I.; Fragai, M.; Luchinat, C.; Parigi, G. Solvent ^{1}H NMRD Study of Hexaaquochromium(III): Inferences on Hydration and Electron Relaxation. *Inorg. Chem.* **2001**, *40*, 4030−4035.
(41) Glass, M. M.; Belmore, K.; Vincent, J. B. Nuclear Magnetic Resonance Studies of Multinuclear Chromium Assemblies. *Polyhedron* **1993**, *12*, 133−140.
(42) Pizzanelli, S.; Kababya, S.; Frydman, V.; Landau, M.; Vega, S. NMR Study of the Adsorption-Desorption Kinetics of Dissolved Tetraalanine in MCM-41 Mesoporous Material. *J. Phys. Chem. B* **2005**, *109*, 8029−8039.
(43) Chen, J. J.; Kong, X.; Sumida, K.; Manumpil, M. A.; Long, J. R.; Reimer, J. A. Ex Situ NMR Relaxometry of Metal-Organic Frameworks for Rapid Surface-Area Screening. *Angew. Chem.* **2013**, *125*, 12265−12268.

https://doi.org/10.1021/acs.jpcc.3c03901
J. Phys. Chem. C XXXX, XXX, XXX−XXX